Best-Fit 3D Phase-Center Determination and Adjustment

Scott T. McBride
David J. Tammen, Ph.D
Doren W. Hess, Ph.D

MI Technologies
1125 Satellite Blvd, Suite 100, Suwanee, GA 30024
smcbride@mitechnologies.com
dtammen@mitechnologies.com

***Abstract*—There are several applications in which knowledge of the location of the phase center of an antenna, and its two-dimensional variation, is an important feature of its use. A simple example occurs when a broad-beam antenna is used as a feed for a reflector, where the center of the spherical phase fronts should always lie at the focal point of the paraboloidal surface. Here, the ability to determine the phase center of the feed from knowledge of its far-field phase/amplitude pattern is critical to the reflector's design.**

Previously published methods process a single cut of data at a time, yielding 2D lateral and longitudinal phase-center offsets. E- and H-plane cuts are thus processed separately, and will, in general, yield different answers for the longitudinal offset. The technique presented here can process either one line cut at a time or a full Theta-Phi raster. In addition, multiple frequencies can be processed to determine the average 3D phase-center offset. The technique can merely report the phase-center location, or it can also adjust the measured phases to relocate the origin to the computed phase center. Example results from measured data on multiple antenna types are presented.

Keywords: Automated phase centering, least-squares fit

I. Introduction

Knowledge of an antenna's phase-center location could have several uses, including:

- determining the phase-center location of a feed antenna or near-field probe relative to a mounting fixture
- determining the change in phase-center location vs. frequency of a broad-band feed or probe
- locating a collection of array elements in the range coordinate system from element-pattern data
- centering the pattern on the phase center so that the phase patterns are more readily interpreted
- automatically determining candidate values for ***IsoFilter™*** [1,2] translations, either for the sake of aligning multiple measurements for self-comparison, or to cause the SNF output to have the origin at the phase center.

Several techniques have been published[3-5] for automatically determining the phase-center location from measured data. The form that comes closest to the approach here is [4], which does a weighted best fit of a single scan's phase with the appropriate bases. This paper presents a separately derived, but functionally equivalent, general algorithm that extends that capability to all three dimensions.

Like many other automated phase-center algorithms, this one makes the important assumption that there is some sizeable region about the AUT's peak where the phase would be constant if the coordinate-system origin were at the phase center. That assumption will generally not be correct for a highly directive antenna.

The phase-center algorithm is available in two places within the MI-3000. The first is an analysis to report the phase-center location(s). The second is a utility that alters the phases of a far-field data file so that the origin is at the coordinates that would be reported by the analysis.

II. Assumptions About AUT Data

A. *Far Field*

Translating the coordinate origin is very straightforward in the far field. Near-field origin translation is far less straightforward, and is typically done by first transforming to the far field. This algorithm assumes that the input data are far-field patterns.

B. *Has a Phase Center Over Non-Zero Region*

This algorithm does not require that the entire antenna pattern have a constant phase when centered. Patterns with side lobes and/or shoulders can be processed, provided that thresholds (defined below) are applied that exclude those features from the processing. It is important, however, that the region being processed have enough samples and angular diversity first to allow the algorithm to run (at least four unique aspects) and then to provide adequate fidelity. For very small regions of θ, the algorithm's bases 1 and K_z will be almost

identical, making the result very sensitive to noise in the measured phase.

C. Adequately Sampled

The sampling required in θ for this algorithm is similar to conventional SNF sampling, where phase change between adjacent samples must be less than 180° (arclength < λ/2):

$$\Delta\theta < \frac{\lambda}{2R_0}\frac{180^0}{\pi}\ , \qquad (1)$$

where R_0 is the radius of the smallest sphere, centered on the axis intersection, containing all radiating sources. This spacing prevents aliasing of the unwrapped phases.

There is no minimum spacing along the ϕ axis. The phase unwrapping is done along the θ axis, with all ϕ angles' phases initially unwrapped at θ=0.

D. Polar Orientation

The MI-3000 implementation restricts the data to include θ=0 in the analyzed region (after angle and amplitude thresholds are applied). This maximizes the fidelity of the 2D phase unwrapping, and also makes the angle and amplitude thresholds much more straightforward to implement. The denser sampling near θ=0 also provides a natural emphasis of the main-beam area in this orientation.

E. Single Co-Polarized Data Bin

The MI-3000 implementation requires that the polarization pattern at θ=0 in the single data bin being analyzed have approximately uniform amplitude and phase. This suggests that the polarization convention be either Ludwig III or circular components.

III. Algorithm

The derivation of this algorithm is extremely simple. We begin with the widespread knowledge that if we translate an antenna by the vector $\vec{R}$, then its far-field pattern $\overrightarrow{P_0}$ before translation will become $\overrightarrow{P_1}$ after translation, with

$$\overrightarrow{P_1} = \overrightarrow{P_0}e^{-j\,\vec{K}\bullet\vec{R}}\ , \qquad (1)$$

where

$$\vec{R} = [x, y, z]$$
$$\vec{K} = [K_x, K_y, K_z].$$

The change in co-polarized phase $\Delta\psi$ due to a translation $[x,y,z]$ (from a centered pattern to the measured orientation) is therefore written simply as

$$\Delta\psi = -(K_x x + K_y y + K_z z). \qquad (2)$$

If a broad-beam antenna has a phase center as defined herein, then the far-field phase over at least its main-beam region should be a constant ψ_o if the phase center is at the origin. We will define $\overrightarrow{P_0}$ in (1) to be this pattern with the centered AUT. The pattern that we measure with the AUT's phase center translated away from the coordinate origin is then $\overrightarrow{P_1}$ in (1). Using the combination of (2), the assumption of constant $\overrightarrow{P_0}$ phase, and the measurement of $\overrightarrow{P_1}$, we can readily (as shown below) determine the vector $\vec{R}$ and/or reconstruct $\overrightarrow{P_0}$ by subtracting $\Delta\psi$ from its phases.

The next thing we need to do is determine the values of K_x, K_y, and K_z corresponding to the measured data. These are readily found from the θ-ϕ aspects of the measured $\overrightarrow{P_1}$ data:

$$\begin{aligned} K_x &= K_0 \sin(\theta)\cos(\phi) \\ K_y &= K_0 \sin(\theta)\sin(\phi) \\ K_z &= K_0\cos(\theta) \end{aligned} \qquad (3)$$

where K_0 is the wave number $2\pi/\lambda$.

We are now ready to form an over-constrained linear system of equations[6], which can be readily solved using any of several linear-algebra libraries. Due to the form of (2), the system of equations we want to solve is

$$\psi(K_x, K_y, K_z) = C_0 + C_1K_x + C_2K_y + C_3K_z, \qquad (4)$$

where $\psi(K_x, K_y, K_z)$ are the unwrapped measured phases at the various aspects of interest. (It is important to note that there is no interpolation from the θ-ϕ grid to a K-space grid. The grid is always that of the acquired data. The least-squares fit operates on a cloud of points, and knows or cares nothing of this grid.)

The matrix form of equations for a weighted least-squares fit can be written as

$$(X^TWX)C = (X^TW)y, \qquad (5)$$

where (in this case)

y is an Nx1 vector of the measured data to be fit

X is an Nx4 matrix of sampled basis functions

W is an NxN diagonal matrix of the sample weights

C is a 4x1 vector with the resulting coefficients

N is the number of data points being fit

4 is the number of sampled basis functions (1, K_x, K_y, K_z).

If an entire sphere were analyzed with uniform weighting ($W \equiv$ identity matrix), then the X^TWX matrix in (5) would become a diagonal matrix due to the orthogonality of the four bases over a full-sphere sample set. In that special case, the determination of the coefficients C from the measured data y would become very straightforward. Any analysis of a partial sphere or any non-uniform weighting, however, requires the more general approach involving either matrix inversion or (preferably) Gaussian reduction[6]. The smaller the effective region analyzed, the less independent will be the four weighted bases over that sample set, and the more sensitive the result to noise in the measured data.

A general note on the least-squares fit: Our bases do not represent a third-order polynomial, but rather a three-dimensional space. Since the matrix equation sees the data and the sampled bases merely as streams of points, there is no distinction between polynomial order and physical dimensions. The bases into the general least-squares fit can therefore be any mix of functions and physical dimensions, provided that they are mutually independent over the sample set. It is up to us to determine useful bases, as we have done in (4).

After forming the matrices and solving this system of equations, the phase-center location is found almost trivially from the best-fit coefficients C_1, C_2, and C_3 as shown in (6):

$$\begin{aligned} x &= C_1 \\ y &= C_2 \\ z &= C_3 \end{aligned} \tag{6}$$

The best-fit constant phase ψ_o is also found as coefficient C_0. This value can be reported and/or subtracted from the data if desired.

A. *Amplitude-Weighting Options*

As Betjes reported[4], weighting the best fit of phase-center locations to the phase data can be beneficial. This weighting de-emphasizes the phase at low signal levels. The MI-3000 implementation of the algorithm offers three options for weighting the least-squares fit:

- Uniform (no weighting)
- Voltage magnitude
- Gain or power (W/W)

The weighting selected will be in addition to any geometric weighting of the sample set. This geometric weighting results from the dense sampling near the pole of the coordinate system.

B. *Amplitude-Threshold Option*

A side lobe in the antenna pattern typically causes a sudden excursion of phase. The inclusion of any side lobes in the pattern being analyzed will therefore violate the assumption that the analyzed region, if relocated to the 'phase center', has approximately constant phase.

This amplitude-threshold option allows the user to restrict the analyzed region with a dB threshold below the peak. For each ϕ angle, data are included in the analysis working outward from θ=0 until the first amplitude on each side (when applicable) drops below the threshold.

C. *Angular-Threshold Option*

This mechanism provides another way for the user to ensure that no side lobes are included in the analysis. Rather than (or in addition to) the amplitude threshold, this restricts consideration to aspects where $|\theta|$ is less than the user-entered value.

D. *Averaging Options*

If an antenna needs to be mounted with its phase center in a certain place, but that phase center wanders with frequency, then some means of combining results over the band will be needed. The software offers a straightforward averaging of each phase-center component over frequency and/or beam.

E. *Single-Scan Processing*

If the data file specified contains a single scan, then the bases K_x and K_y are combined into a single basis K_{xy}, such that the algorithm yields a lateral and a longitudinal offset. Except for the added data-exclusion options, this processing should be equivalent to the single-scan analysis in [4].

IV. DATA

A. *Gain Standard*

A standard gain horn (SGH) is one type of antenna that does not have a true phase center beyond its main-beam peak. Here we process spherical near-field (SNF) data acquired in a large arch-based system[7]. The SGH, shown in the range in Figure 1, was intentionally offset in all dimensions from the axis intersection. The black dot in Figure 1 is the approximate location of the phi axis of rotation at the absorber level. For the purpose of this demonstration, the SNF data on this horn have been transformed to the far field, and then rotated so that the peak is pointing along the Z axis. The resulting far-field amplitude and phase patterns (in the Ludwig III polarization convention) are shown in Figure 2 and Figure 3.

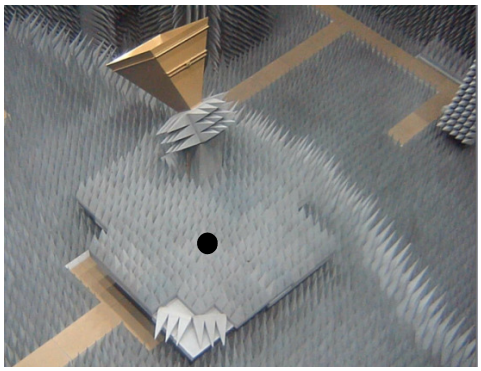

Figure 1. Offset Gain Standard

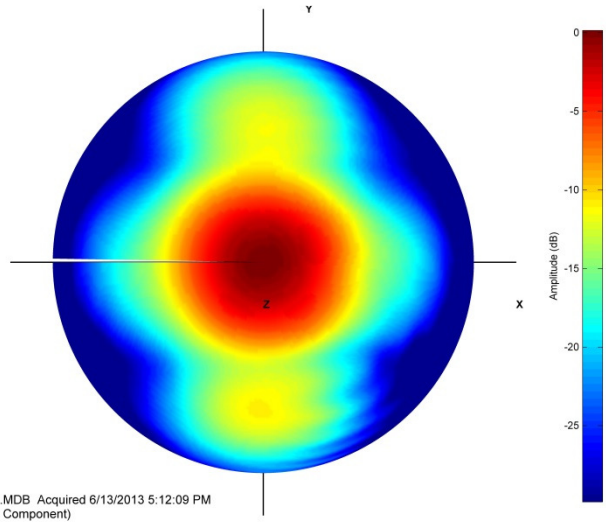

Figure 2. SGH amplitude pattern

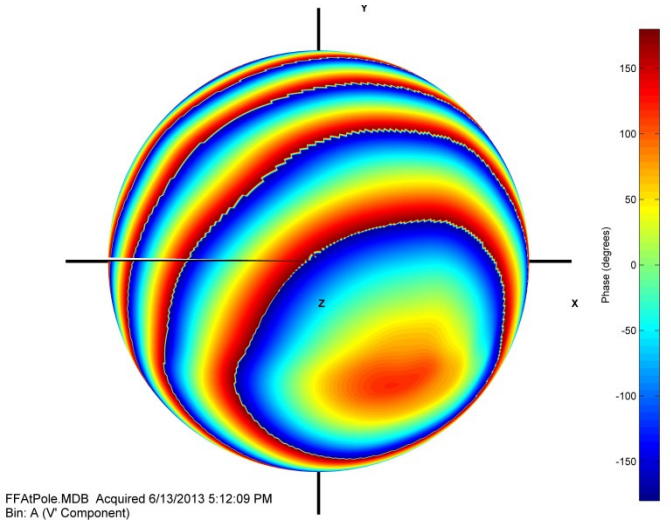

Figure 3. Phase plot of offset SGH

Figure 4 shows the intermediate stage (incorporated in the analysis) of unwrapping the phase prior to the least-squares fit. Note that the phase scale has changed from 360° to over 1700°.

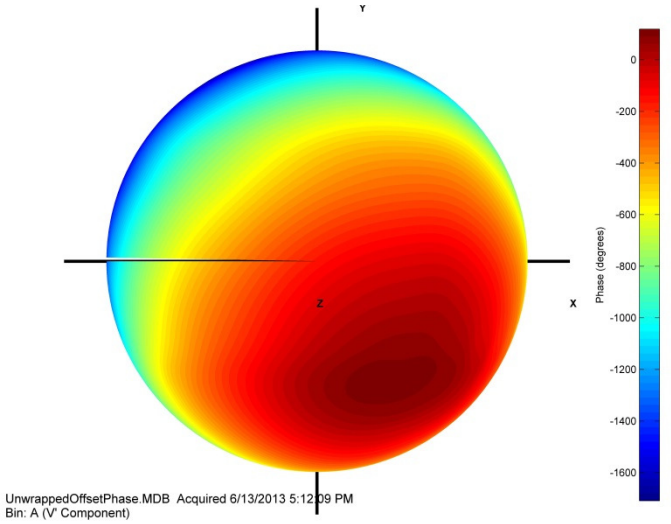

Figure 4. Unwrapped SGH Phase

We begin our analysis of this data by running this far-field data set through the MI-3000's phase-center analysis. To avoid the SGH shoulders, the angular threshold was set to $|\theta| \leq 20°$. The results (in inches) are shown in Figure 5.

We then entered those values in as the MI-3046 SNF software's ***IsoFilter***™ [1,2] translations and re-transformed from the far field to the far field. The post-centering phase returned from the analysis was also entered as the MI-3046 phase offset. The resulting phase is shown in Figure 6. A black circle has been superimposed on Figure 6 to show the 20° angular threshold used in the phase-center determination. As expected, the phase inside that circle has become flat and zero-mean in a best-fit sense.

MI-3000 Analysis Results

Value being computed	*Min*	*Result*	*Max*
Phase Center Analysis			
Phase Center Location X:		**29.08**	
Phase Center Location Y:		**-39.93**	
Phase Center Location Z:		**62.28**	
Post-Centering Phase:		**114.92**	

Phase Center Analysis of file FFAtPole.MDB on the A (V' Component) channel

Figure 5. Phase-center analysis results

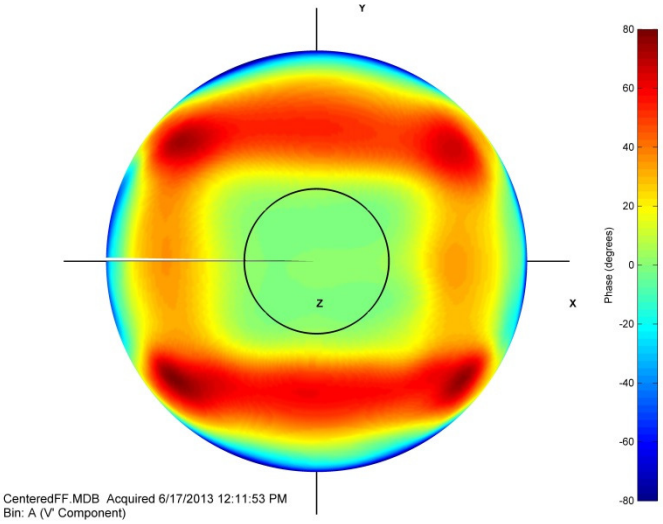

Figure 6. Phase plot of numerically centered SGH

For comparison, we re-processed the same data specifying a $|\theta|$ threshold of 45° to include portions of the phase ridges seen in Figure 6. The resulting phase (along with the 45° threshold) is shown in Figure 7, plotted on a ±30° scale. We see in Figure 7 that the phase in the specified region has been flattened in a best-fit sense, but that it is not nearly as flat as that in Figure 6. The reported x and y locations of the phase center each changed by less than $\lambda/500$, but the z location changed by 0.27λ due to this change in angular threshold. Note that no amplitude weighting was specified, but that the geometric weighting (due to denser sampling near the peak) has driven the peak phase to be flatter than the edge phase.

The shape of the main-beam phase in Figure 7 indicates that if the centered main-beam phase is expected to be constant, then a tighter angular (or amplitude) threshold is required.

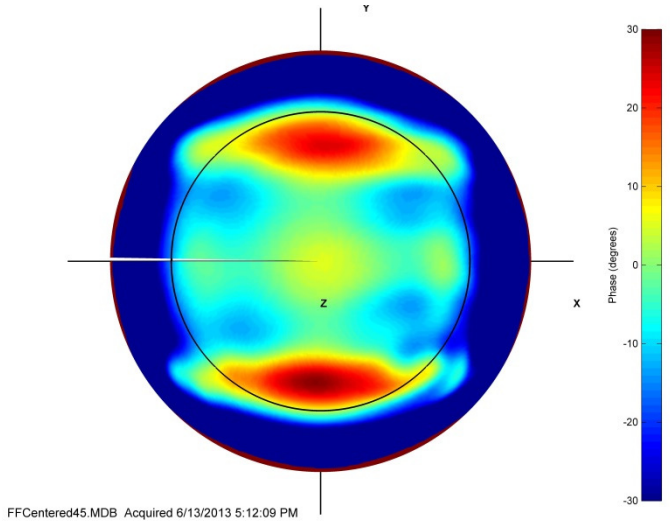

Figure 7. SGH phase with 45° θ threshold

B. *Log-Periodic Dipole Array*

A log-periodic array (LPA) achieves broad-band performance by using different active dipole elements at different frequencies. As one would expect, the phase center of the LPA changes with frequency based on the location(s) of the active dipole(s).

The measured data for an MI-26-0.35 LPA were processed in the MI-3000's phase-center analysis, with results plotted in Figure 8. We see the expected variation of phase-center location in Z vs. frequency, as well as some minor perturbations in X and Y.

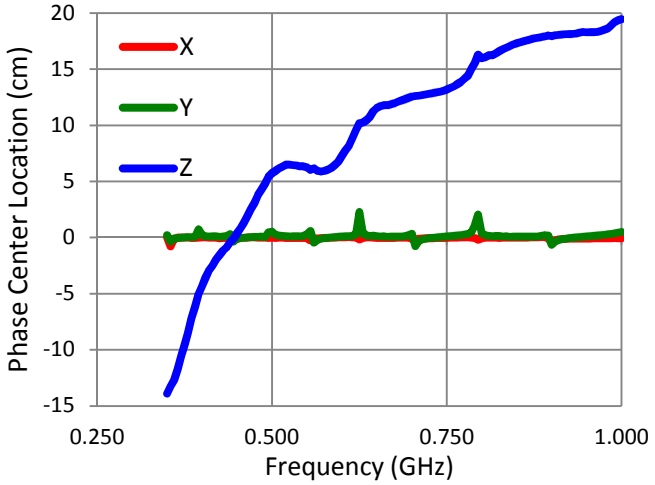

Figure 8. LPA phase center vs. frequency

C. *Small Horn Over Absorber*

This antenna exhibits a phenomenon that is often seen in phase centering, where the E plane and H plane disagree on where the phase center ought to be [4,5,8]. This disagreement leads to a saddle shape in the phase pattern of the 'centered' antenna.

The horn was measured over an absorber-covered ground plane. It has a very broad beam, shown in Figure 9.

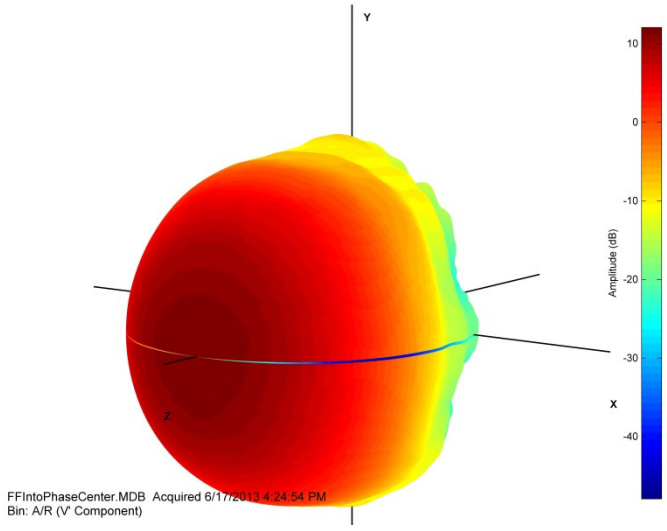

Figure 9. Small horn amplitude

The horn was offset from the axis intersection, and its phase pattern is shown in Figure 10. One can see from the striping of the phase pattern that the dominant translation will be along the Y axis. The horn pattern was passed into the phase-center analysis (for illustration purposes only), and the results are shown in Figure 11.

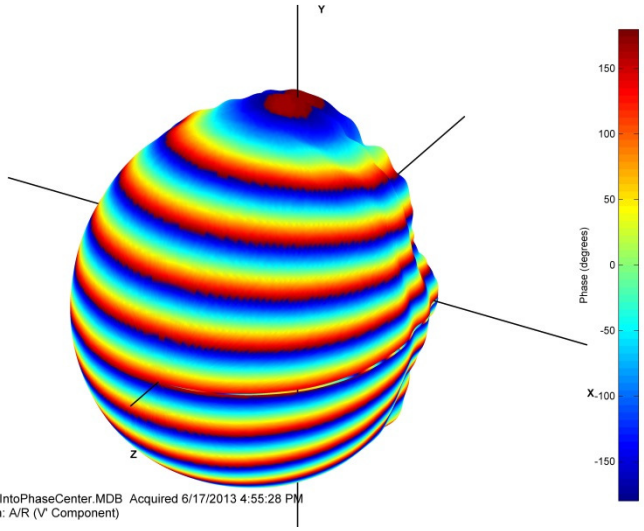

Figure 10. Small horn phase

MI Technologies

MI-3000 Analysis Results

Value being computed	*Min*	*Result*	*Max*
Phase Center Analysis			
Frequency: 8 GHz			
Phase Center Location X:		**-0.10**	
Phase Center Location Y:		**-7.94**	
Phase Center Location Z:		**-0.42**	
Post-Centering Phase:		**-105.02**	

Phase Center Analysis of file FFIntoPhaseCenter.MDB on the A/R (V' Component) channel

Figure 11. Small horn phase-center results

Instead of manually entering these numbers into the MI-3046 SNF software, we ran the same file through the MI-3000's phase-centering application. This computes the translations and implements them in one step. A $|\theta| \leq 30°$ cutoff was specified, and the resulting phase (on a ±10° color scale) is shown in Figure 12. The saddle shape is very evident in Figure 12, where the phase goes up with |Y|, and down with |X|.

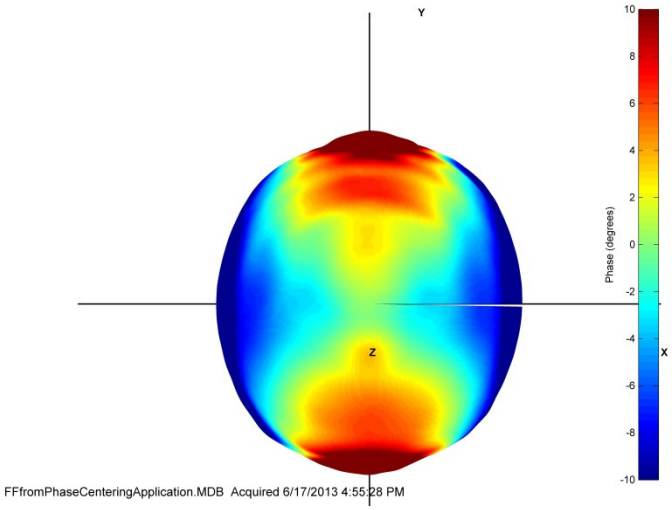

Figure 12. Small horn centered phase

One perceived advantage of this 3D phase-centering algorithm is that it finds the best-fit location from all the specified data, removing any guesswork from balancing the two planes. Figure 13 shows the phase along the principal planes within the ±30° range of θ used for the best fit.

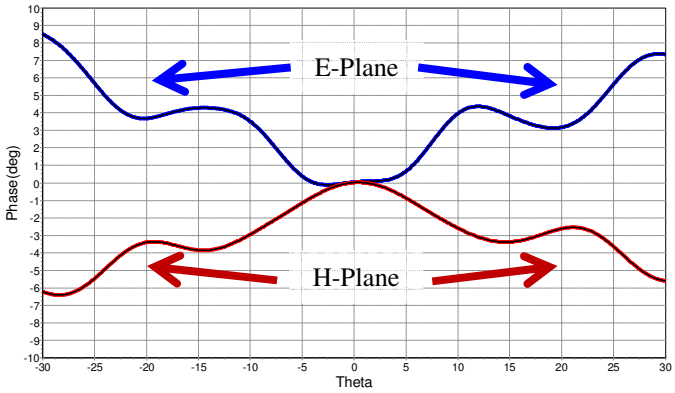

Figure 13. Small horn principal-plane phase

V. Conclusions

A new general algorithm for locating the phase center of a broad-beam antenna has been introduced and implemented. It provides user control over the processing to avoid problem areas like side lobes, shoulders, and low signal levels. The coordinate origin can also be automatically translated to the phase center, and then the meaningful details of the phase pattern can be more readily observed. The guesswork in balancing the 'saddle' of a horn's distorted phase is removed by finding that balance in a least-squares sense over the entire specified 3D pattern. The phase center's computed coordinates can be used to show the frequency migration of its location and/or the locations of multiple individually radiating elements.

Acknowledgements

The authors would like to acknowledge the late Dr. Doren Hess for, among other things, his statement of the problem, early research into existing methods, ideas for side-lobe restriction, and critique of the algorithm.

References

[1] D. W. Hess, "The ***IsoFilter***™ technique: isolating an individual radiator from spherical near-field data measured in a contaminated environment", Post-Deadline Paper, AMTA 2006, Austin TX.

[2] D. W. Hess, "The ***IsoFilter***™ technique: extension to transverse offsets", Post-Deadline Paper, AMTA Proceedings, Austin, 2006.

[3] P. Kolesnikoff, "Phase center location and stability of wide beam GPS antennas", AMTA Proceedings, pp. 1-25-1-30, Boulder, October, 1991.

[4] P. N. Betjes, "An algorithm for automated phase center determination and its implementation", AMTA Proceedings, pp. 190-195, St. Louis, November, 2007.

[5] S. Pivnenko, "Using the phase center of a standard gain horn in antenna gain determination", AMTA Proceedings, pp. 334-340, Boston, 2008.

[6] S. D. Conte, C. de Boor, Elementary Numerical Analysis: an Algorithmic Approach, 3rd ed., Ch. 4, McGraw-Hill, 1980.

[7] S. T. McBride, J. P. Marier, C. J. Kryzak, J. Fordham, K. Liu, "A large spherical near-field arch scanner for characterizing low-frequency phased arrays", AMTA Proceedings, pp. 293-298, Englewood, October, 2011.

[8] E. I. Muehldorf, "The phase center of horn antennas", IEEE Trans. Antennas Propagat., vol. AP-18, no. 6, pp. 753-760, Nov. 1970.